Platinum-group and noble metals under oxidizing conditions

2008 J. Phys.: Condens. Matter 20 184023

(http://iopscience.iop.org/0953-8984/20/18/184023)

J. Phys.: Condens. Matter **20** (2008) 184023 (11pp) doi:10.1088/0953-8984/20/18/184023

Platinum-group and noble metals under oxidizing conditions

N Seriani and F Mittendorfer

Faculty of Physics, Universität Wien, and Center for Computational Materials Science, Sensengasse 8/12, A-1090 Vienna, Austria

E-mail: nicola.seriani@univie.ac.at

Received 1 August 2007
Published 17 April 2008
Online at stacks.iop.org/JPhysCM/20/184023

Abstract

Platinum-group metals and noble metals play an important role in catalysis, for total oxidation as well as for partial oxidation reactions. Only in recent years have advances in microscopic, spectroscopic and computer simulation techniques made it possible to investigate the interaction of oxygen with metallic substrates at an atomistic level. We present an overview on the formation of adsorption structures and surface oxides on Rh, Pd, Ag, Cu and Pt surfaces, with particular focus on the phase diagrams calculated from first-principles thermodynamics. The low-index (111), (100) and (110) surfaces as well as selected high-index surfaces have been considered. We predict the stability of novel structures such as the c(4 × 6) on Cu(100) and the α-PtO_2 trilayer on Pt(100). The knowledge of the Gibbs free surface energies allows us to predict the adsorbate-induced changes in the thermodynamic equilibrium shape of metal nanoparticles. At low oxygen chemical potential, corresponding to clean surfaces, the (111) facets dominate the particle shape, with a significant contribution from (100) facets. But even under these conditions a small fraction of the overall surface corresponds to more open facets. As oxygen adsorption sets in, their contribution becomes larger. At high oxygen partial pressures, surface oxides form on the platinum-group metals. They do not only display different chemical properties than the metal, but also determine the exposed surface orientations of the particles. The latter effect might play an important role for the catalytic activity of transition metal nanoparticles.

1. Introduction

Platinum-group metals and noble metals are the main active components in heterogeneous oxidation catalysts, where they are usually applied in the form of nanoparticles on a ceramic (oxidic) support [1]. Their applications span a wide range from catalytic converters for the treatment of automotive exhaust [2] to catalysts for the production of fine chemicals. Important differences in activity and selectivity exist among individual metals. Rhodium, platinum and palladium are excellent catalysts for total oxidation of hydrocarbons and carbon monoxide. In addition, an important role of rhodium in PtRh catalysts is to reduce nitrogen oxides, due to its ability to dissociate NO [2, 3]. On the other hand, Ag and Cu are mainly used for partial oxidation reactions [4, 5], such as ethylene epoxidation, conversion of methanol to formaldehyde and partial oxidation of methanol.

While investigations of well-defined transition metal surfaces under ultrahigh vacuum (UHV) have been viable for decades, these systems differ in important aspects from the technologically used catalysts. On one hand, adsorbates like oxygen modify the chemical properties of surfaces; on the other hand, a single-crystal surface has a low density of defects in comparison to a metal nanoparticle (pressure and materials gap). Only in recent years have advances in microscopic, spectroscopic and simulation techniques made it possible to characterize metal surfaces under high oxygen pressure. This has led to the discovery and characterization of several monolayer-thin surface oxides [6–17]. Still, to our knowledge, for many of the metals mentioned only incomplete data are available. For instance, on Pt(100) the formation of an oxide layer starting at an oxygen coverage of 1 monolayer (ML) was measured after exposing the surface to a beam of atomic oxygen [18], but its atomic structure has not been resolved. One of the authors of this paper has predicted a PtO monolayer to be the stable (2 × 2) oxide monolayer, while with progression of the oxidation a Pt_3O_4 film would become more stable thanks to a stress-free interface [19].

Even in cases where the existing surface oxides have been thoroughly investigated, their catalytic activity has seldom been characterized. Frenken and co-workers found the surface oxides to be catalytically more active towards CO oxidation than the metallic phases of Pt(110) [20, 21], suggesting a Mars–Van Krevelen mechanism for CO oxidation [22]. For Pd(100), kinetic Monte Carlo simulations based on parameters deduced from *ab initio* calculations suggested that, under the typical conditions at which CO oxidation takes place, the surface oxide might be present and subject to continuous cycles of formation and reduction [23]. For Ag the hypothesis that Ag_2O or Ag with subsurface oxygen are the active phase was put forward [24].

Besides changes in the chemical activity of surfaces, oxygen is also responsible for shape changes in metal particles with respect to UHV conditions, as shown for example by transmission electron micrographs of Pd particles [25, 26]. Although particle shapes have been investigated for decades [25–33], we are only aware of a few studies on the equilibrium shape of Pd particles in an oxygen rich atmosphere [25, 26]. To our knowledge a systematic assessment of the dependence of the equilibrium shape on oxygen pressure and temperature is still missing. An important step in this direction is to understand which oxygen structures form at metal surfaces, and how they influence the shape of metal nanoparticles.

We have conducted first-principles simulations of low-index and selected stepped surfaces for Rh, Pd, Pt, Ag and Cu, and calculated the dependence of the phase diagrams for each surface on the chemical potential of oxygen in the framework of first-principles thermodynamics. We have then employed this information to predict the shape of particles in thermodynamic equilibrium, from UHV to high oxygen pressure conditions, by means of the Gibbs–Wulff construction. In section 2 the computational methods are reported, in section 3 results on oxygen adsorption on single-crystal surfaces are discussed, and in section 4 the resulting morphological changes of metallic nanoparticles are presented. For the sake of brevity, we report surface phase diagrams and atomic structures only for facets and structures that are presented here for the first time, indicating literature references for the others.

2. Computational methods

First-principles calculations were performed within density functional theory (DFT) with the Vienna *Ab initio* Simulation Package (VASP) [34], using the projector-augmented wave method (PAW) [35, 36]. The exchange–correlation energy was expressed within the generalized gradient approximation (GGA) in the PW91 formulation [37]. An energy cutoff of 250 eV was employed, with the exception of Cu, where a cutoff energy of 275 eV was used. Brillouin zone integration was performed using Monkhorst–Pack grids [38] corresponding to a (16 × 16× 1) grid in the p(1 × 1) surface cell. We used the theoretical lattice constants of 3.98 Å for Pt (experimental 3.92), 3.95 Å for Pd (exp. 3.89), 3.84 Å for Rh (exp. 3.80), 4.16 Å for Ag (exp. 4.09), and 3.64 Å for Cu (exp. 3.61). The respective surface orientations have been modeled by periodically repeated slabs, consisting of six metal layers for the close-packed (111) layers, and eight layers for the more open (100) and (110) surfaces. For the stepped surfaces six layers parallel to the (111) terraces have been used. Relaxation of all atoms but those in the 2–4 lowest layers was performed by damped molecular dynamics until the forces on the atoms became smaller than 0.02 eV $Å^{-1}$.

In the present work, the Gibbs free surface energy is calculated from *ab initio* thermodynamics [39] as

$$\gamma(\mu_M, \mu_O) = (E_{tot} - N_M\mu_M - N_O\mu_O)/A - \gamma_{clean} \quad (1)$$

with the total slab energy E_{tot}, the number of metal (oxygen) particles N_M (N_O) and the surface area A. The surface energy of the clean surface, γ_{clean}, is subtracted because of the asymmetric setup used in the calculations. The chemical potential of the metal atoms, μ_M, is approximated by the binding energy of the bulk phase, and the vibrational contributions of adsorbates and substrate have been neglected [19, 39].

The shape of an unsupported nanoparticle at thermodynamic equilibrium can be obtained from the Gibbs–Wulff construction [40]. The Gibbs surface free energy G can be written as $G = \sum \gamma_i A_i$, where A_i are the facet areas and γ_i the corresponding surface energies. According to the Wulff construction, the crystal shape that minimizes the free energy G at constant volume has a constant ratio between the surface energy γ_i and the distance d_i of the corresponding basal plane to the center of the particle:

$$\gamma_i/d_i = \text{const.} \quad (2)$$

In the Wulff construction the energy contributions from the particle edges are neglected, and thus the resulting shape is size-independent. Since this method is not valid for small particles [41], their shape might deviate from the predictions; experimental data indicate that particles in the range of tens of nanometers are already consistent with this construction principle [27, 28]. Molecular dynamics simulations of copper nanoparticles have shown that the Wulff shape is the equilibrium shape for particles larger than 3.8 nm [42]. We have used this method, taking into account the three low-index surfaces and selected stepped surfaces, namely (211), (311) and (331). For the clean surfaces, other facets such as (210) and (411) change the general conclusion only a little.

3. Surfaces

3.1. Clean surfaces

In table 1 we report the energies of the clean, unreconstructed surfaces. The results are in agreement with previously published data [43–45]. For the 4d metals considered, a steady decrease in the surface energy from Rh to Ag is predicted. The large difference in the absolute values of the surface energies γ conceals an approximate regularity that is evident as soon as the surface energies are expressed in units of the respective $\gamma(111)$ (see table 2). For each facet, this ratio is consistent

Table 1. Surface energies of clean unreconstructed surfaces (in eV Å^{-2}). For Pt(100), Pt(110) and Pt(311) the surface energies of reconstructed phases are reported as well. Missing-row reconstructed structures are indicated by (MR).

Structure	Rh	Pd	Ag	Cu	Pt
(111)	0.124	0.084	0.047	0.082	0.093
(100)	0.144	0.094	0.052	0.090	0.113 ((1 × 5): 0.098)
(110)	0.147	0.099	0.055	0.096	0.123 ((1 × 2)-MR: 0.103)
(331)	0.143	0.095	0.053	0.092	0.105
(311)	0.148	0.098	0.052	0.092	0.110 (MR: 0.108)
(211)	0.144	0.095	0.053	0.092	0.103

Table 2. Ratio of surface energies $\gamma_X/\gamma(111)$.

Structure	Rh	Pd	Ag	Cu	Pt	BB model
(100)	1.17	1.12	1.11	1.10	1.22 ((1 × 5): 1.05)	1.16
(110)	1.19	1.18	1.18	1.16	1.32 ((1 × 2)-MR: 1.11)	1.22
(331)	1.16	1.13	1.14	1.12	1.12	1.19
(311)	1.20	1.16	1.12	1.13	1.19 (MR: 1.16)	1.13
(211)	1.17	1.13	1.13	1.12	1.11	1.18

within 8% with a bond-breaking (BB) model, a fact which has also been observed for other metals [46, 47]. The deviations from the BB model, though small, are responsible for the stability of faceted surfaces in the Wulff construction [48–50].

For Pt(100) and Pt(110) we report surface energies for both unreconstructed and reconstructed surfaces. These two surfaces are known to reconstruct in the absence of adsorbates: (110) in the (2 × 1) missing-row structure [51], and (100) in three different structures: (1×5) [52], Pt(100)-hex and the most stable Pt(100)-hexR0.7° [53, 54]. For computational reasons, we have simulated only the (1 × 5) reconstruction, which has a very similar structure to the other two, with a Pt overlayer in hexagonal arrangement over the (100) surface. Consistently, both reconstructions on Pt(100) and on Pt(110) make the two surfaces more similar to a (111) surface: the reconstruction on (100) by creating an overlayer with hexagonal coordination, and the reconstruction on (110) by exposing broader (111) terraces.

3.2. Oxygen adsorption

The adsorption of oxygen on single-crystal surfaces has been a major topic of surface science studies in the last decades. Although the detailed description of each single adsorption phase is beyond the scope of this paper, we will give a brief overview of the common aspects in the present section.

Comparing the adsorption of oxygen on the close-packed (111) surfaces, the differences between noble metals and platinum-group metals become evident. The platinum-group metals form simple p(2 × 2) adsorption structures in a first step. On the other hand, for noble metals it seems that undercoordinated metal atoms at the surface, like adatoms, are necessary to allow for oxygen adsorption on the close-packed (111) surface [12, 13, 15, 16]. These complex structures, involving major surface reconstructions, are often classified as surface oxides, since their stoichiometry and metal coordination is that of Ag_2O and Cu_2O, respectively. These

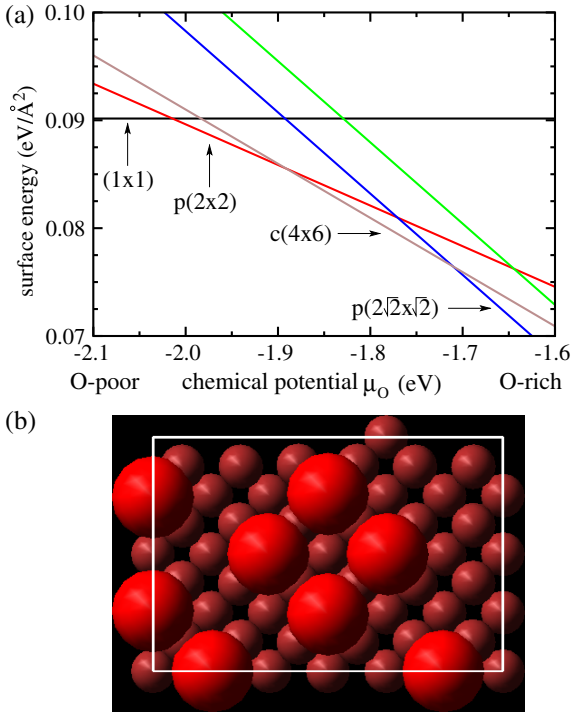

Figure 1. (a) Surface phase diagram for Cu(100). Black line: clean Cu(100); red line: p(2 × 2); green line: c(2 × 2); blue line: p(2$\sqrt{2}$ × 2)R45°-O; brown line: c(4 × 6). (b) Atomic structure of the c(4 × 6) phase; large red spheres: O atoms; small red spheres: Cu atoms; white line: elementary surface cell.

structures will be described in section 3.3. Oxygen adsorption is not very favorable on the noble metal (111) surfaces for kinetic reasons (formation of the stable phase requires reconstruction of the surface and appearance of adatoms); additionally, on Ag(111) there is also a low adsorption energy.

For the (100) surface, most of the metals considered display an interval of stability for the p(2 × 2)-1O structure, with oxygen atoms adsorbed in the fourfold-coordinated hollow site. While this structure is stable on Pd(100) up to the formation of the surface oxide (see section 3.3), it is replaced by a c(2 × 2)-1O reconstructed structure on Rh(100) at a higher coverage [55, 56]. For the adsorption on Pt(100), the picture is more complex. The (1 × 5) reconstruction of the *clean* surface is lifted by O adsorption [57]. This experimental observation is confirmed by our calculations: the hypothetical adsorption of oxygen on the (1 × 5) reconstruction is very weak. Lifting the reconstruction is so expensive that at least a coverage of 0.5 ML oxygen is required. In this case a p(2 × 1) phase forms, with oxygen adsorbed in bridge sites, and it is stable until the chemical potential approaches the bulk oxide phase (see figure 2(a)). For both Ag(100) and Cu(100) we predict a transition from the p(2×2) to the c(4×6) structure at an oxygen coverage of 1/3 ML (figure 1). While this structure has been observed on Ag [14], we are not aware of any experimental confirmation on Cu(100).

Under oxidizing conditions, (110) surfaces of all platinum-group metals show a tendency to undergo a missing-row reconstruction. In the prototypical case of Rh(110),

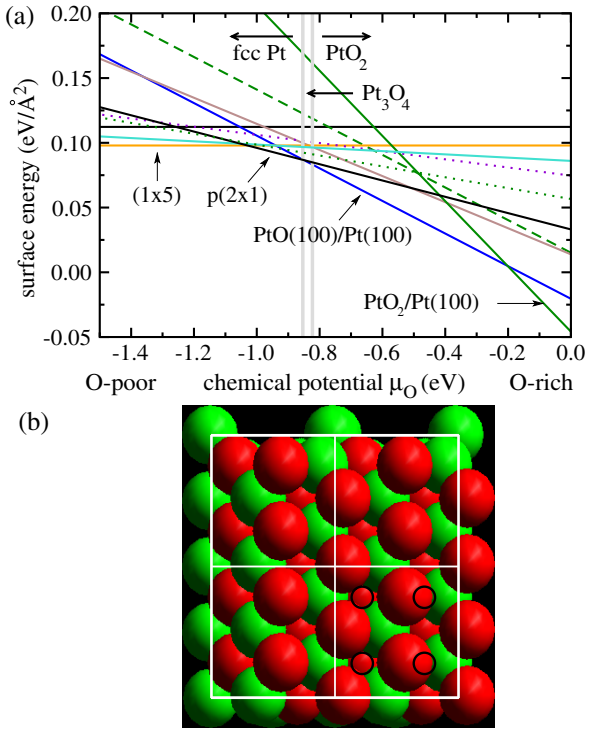

Figure 2. (a) Surface phase diagram for Pt(100). Horizontal black line: clean unreconstructed Pt(100); orange line: clean (1 × 5) reconstruction; dotted violet line: p(2 × 2) on unreconstructed surface; turquoise line: 0.1 ML oxygen on the (1 × 5) reconstruction; blue line: PtO(100)@Pt(100); brown line: $(\sqrt{5} \times \sqrt{5})$R27° structure, i.e. PtO(101)@Pt(100); green solid line: α-PtO_2(0001)@Pt(100); green interrupted line: Pt_3O_4(100)@Pt(100); black line: p(2 × 1); green dotted line: p(3 × 1). The grey vertical lines indicate the intervals of stability of the bulk phases. (b) Atomic structure of the α-PtO_2(0001)@Pt(100) phase; red spheres: O atoms; green spheres: Pt atoms; white line: (2 × 2) surface cell; black circles: topmost Pt atoms of the substrate.

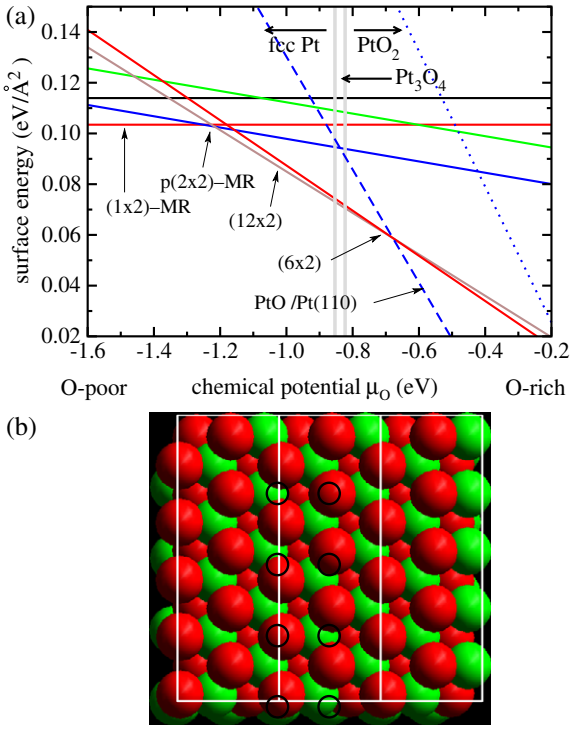

Figure 3. (a) Surface phase diagram for Pt(110). Black line: clean unreconstructed Pt(110); red horizontal line: clean (1 × 2)-missing row (MR) reconstruction; solid blue line: p(2 × 2) on (1 × 2)-MR; green line: p(2 × 2) on the unreconstructed surface; brown line: (12 × 2); red line: (6 × 2); blue interrupted line: α-PtO_2(0001)@Pt(110)-(2 × 4); blue dotted line: α-PtO_2(0001)@Pt(110)-(1 × 4). The grey vertical lines indicate the intervals of stability of the bulk phases. (b) Atomic structure of the α-PtO_2(0001)@Pt(110)-(2 × 4) phase; red spheres: O atoms; green spheres: Pt atoms; white line: (2 × 4) surface cell; black circles: topmost Pt atoms of the substrate.

we find that a p(2 × 2)*p2mg* structure and variants thereof are stable at a coverage of 0.5 ML [58], in agreement with experimental observation [59–62]. The basic structure of this phase is a zig-zag arrangement of oxygen atoms adsorbed in hollow sites at the step edge of the missing-row reconstructed surface. On Pt(110) our calculations show that the only stable adsorption phase has a p(2 × 2) periodicity with 0.25 ML oxygen adsorbed in threefold sites along the topmost Pt rows on the missing-row surface (figure 3(a)), while the (2 × 2)*p2mg* phase is only metastable. Finally, on Pd(110) a large variety of structures has been observed, among them p(1 × 2), c(2 × 4), c(2 × 6), (2 × 3)-1D, (3 × 2) and a 'complex' structure [63–66]. At the onset of adsorption we find [66] a small interval of stability of the (2 × 3)-1D proposed by Comelli and co-workers [67]. Then the c(2 × 4) phase is stable in a wide region of the chemical potential. Yet the related (2 × 2)*p2mg* structure, differing from the c(2 × 4) because every second oxygen zig-zag row is mirrored, is energetically nearly degenerated with the c(2 × 4). The situation is much simpler for the noble metals Ag and Cu, where a (2 × 1)-added row structure is the only stable adsorption structure at 0.5 ML coverage (see figures 4 and 5).

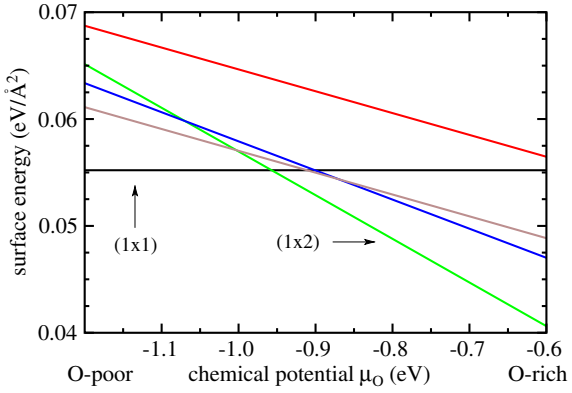

Figure 4. Surface phase diagram for Ag(110). Black line: clean Ag(110); green line: clean (2 × 1)-added row structure; blue line: (3 × 1)-added row structure; brown line: (4 × 1)-added row structure; red line: p(2 × 2).

For the stepped surfaces, experimental data about oxygen adsorption is rather scarce. Therefore, as long as not mentioned otherwise in the text, we have chosen the basic adsorption structures introduced for the (110) surface as structural models. The stepped face-centered cubic (fcc) (331) surface possesses

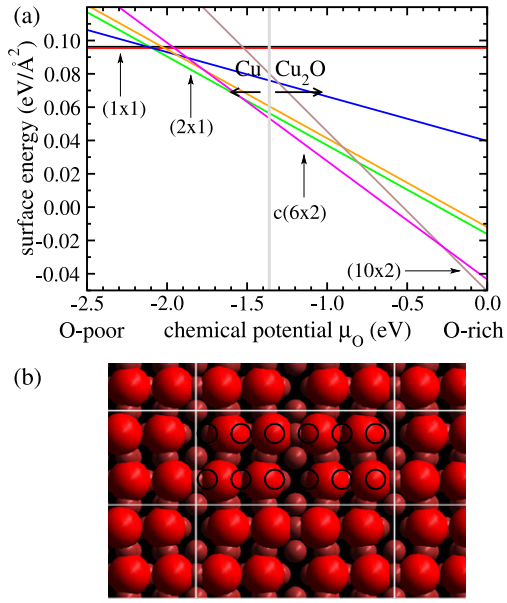

Figure 5. (a) Surface phase diagram for Cu(110). Black line: clean unreconstructed Cu(110); red line: clean (1 × 2)-missing row reconstruction; green line: (2 × 1)-added row structure; blue line: (4 × 1)-added row structure; orange line: c(2 × 4); magenta line: c(6 × 2); brown line: (10 × 2). The grey vertical line indicates the intervals of stability of the bulk phases. (b) Atomic structure of the c(6 × 2) phase; large red spheres: O atoms; small red spheres: Cu atoms; white line: elementary surface cell; black circles: Cu atoms in the topmost layer of the substrate.

Table 3. Stable adsorption phases of oxygen on Pt, Rh and Pd surfaces. The adsorption energies are given with respect to the unreconstructed surface. Missing-row reconstructed structures are indicated by (MR). Structures with O adsorbed at bridge positions are indicated with bri. For stepped surfaces, low-coverage oxygen adsorption is indicated as 1O, '$p2mg$'-like structures as 2O, and oxide stripes as 4O. E_{ads} is the average adsorption energy with respect to the clean unreconstructed surface.

Structure	E_{ads} (eV)	Structure	E_{ads} (eV)
Pt(111) p(2 × 2)	−1.25	Pt(111) PtO_2	−0.77
Pt(100) p(2 × 2) bri	−1.19	Pt(100) p(3 × 1) bri	−1.32
Pt(100) p(2 × 1) bri	−1.25	Pt(100) PtO(100)	−1.05
Pt(100) PtO_2	−0.63	Pt(110) p(2 × 2) (MR)	−1.25
Pt(110) (12 × 2)	−1.23	Pt(110) PtO_2 (2 × 4)	−0.88
Pt(331) 1O	−1.27	Pt(331) 2O	−1.07
Pt(331) 4O	−0.99	Pt(311) 1O	−1.47
Pt(311) 2O	−0.81	Pt(211) 1O	−1.43
Pt(211) 2O	−1.02	Pt(211) 4O	−0.63
Rh(111) p(2 × 2)	−2.05	Rh(111) p(2 × 1)	−1.80
Rh(100) p(2 × 2)	−2.26	Rh(100) c(2 × 2)	−2.08
Rh(110) p(2 × 2)$p2mg$	−2.25	Rh(110) c(2 × 6)	−2.07
Rh(110) c(2 × 8)	−1.99	Rh(110) c(10 × 2)	−1.89
Rh(331) 1O	−2.19	Rh(331) 2O	−2.02
Rh(331) p(10 × 1)	−1.71	Rh(311) 1O	−2.19
Rh(311) 2O	−1.80	Rh(211) 1O	−2.22
Rh(211) 2O	−1.93	Rh(211) 4O	−1.45
Pd(111) p(2 × 2)	−1.36	Pd(100) p(2 × 2)	−1.38
Pd(110) p(2 × 3)	−1.56	Pd(110) c(2 × 4)	−1.53
Pd(331) 1O	−1.44	Pd(331) 2O	−1.38
Pd(311) 2O (MR)	−1.45	Pd(311) (1 × 2) (MR)	−1.04
Pd(211) 1O	−1.26	Pd(211) 2O	−1.23

a two-atom wide (111) terrace and a monoatomic (111) faceted step. The adsorption of oxygen on Rh(331) has been studied in detail experimentally and theoretically [68]. In the low-coverage case, the oxygen adsorption starts in the undercoordinated hexagonal close-packed (hcp) hollow site at the upper step edge. Compared to Rh(111), the adsorption energy is enhanced by about 10% (see table 3). At an increasing coverage the generally repulsive interaction between the adsorbates suppresses the formation of a p(2 × 1) line-wise structure on the terraces and leads to a zig-zag, '$p2mg$'-like arrangement at the step. This arrangement is usually stable over a wide pressure regime. Finally, if the oxygen partial pressure is high enough to overcome the nearest-neighbor repulsion, the step is fully covered with oxygen forming one-dimensional stripes [48]. A similar pattern is found for all transition metals presented in this work. For Pd(331), the $p2mg$ zig-zag phase is exceptionally stable (see table 3), and therefore present in a wide range of the phase diagram, reaching well into the stability of the bulk oxide. The opposite effect can be observed for Pt(331), where neither the $p2mg$ nor the p(2 × 1) phase are stable, and at a chemical potential of $\mu = -0.9$ eV a direct transition from the monoatomic low-coverage phase to the fully covered step is predicted. On the other hand, the two noble metals Cu and Au follow the trend for Pd, that is the monoatomic adsorption is either unstable (Ag) or only stable in a small region of the phase diagram (Cu), while the $p2mg$-like structure is stable up to a pressure regime close to the bulk stability of the oxides (see figures 6(d) and (e)).

The situation is much less uniform for the transition metal (311) surfaces. The structure of the fcc (311) surfaces is similar to the fcc (110) surface, but instead of two (111) facets an alternating arrangement of (111) and (100) facets is present. Due to the high step density the (311) surface is prone to adsorbate-induced reconstructions. Consequently, we do not only present the data for oxygen adsorption for the simple (311) surfaces, but also on the missing-row (MR) reconstructed surfaces. On Rh(311), the low-coverage adsorption energy is nearly the same as on Rh(331), $E_{ads} = -2.2$ eV, but the preferred adsorption site changes from a hollow site to a bridge site at the step edge. At higher oxygen coverage the formation of a zig-zag pattern along the step edge has recently been observed [69], but this structure is significantly less stable than on Rh(331), and consequently only exposed in a relatively small regime of the phase diagram, ranging from $\mu = -1.4$ to -1.2 eV. A transition to the Rh surface oxide trilayer, discussed in section 3.3, would only take place in the stability regime of the bulk oxide. For Pd(311) the energetic cost for a missing-row reconstruction is very low. In contrast to Rh, we find that the zig-zag arrangement of the oxygen atoms along the step alternating in threefold and fourfold hollow sites is very stable. In fact, this arrangement on the MR reconstructed surface is the only thermodynamically stable adsorption phase on Pd(311) before entering the bulk oxide regime. Like in the case of Rh(311), the adsorption of a single oxygen atom at a bridge site on Pt(311) is strongly stabilized compared to the low-indexed Pt(111) surface. Yet, at a higher coverage the

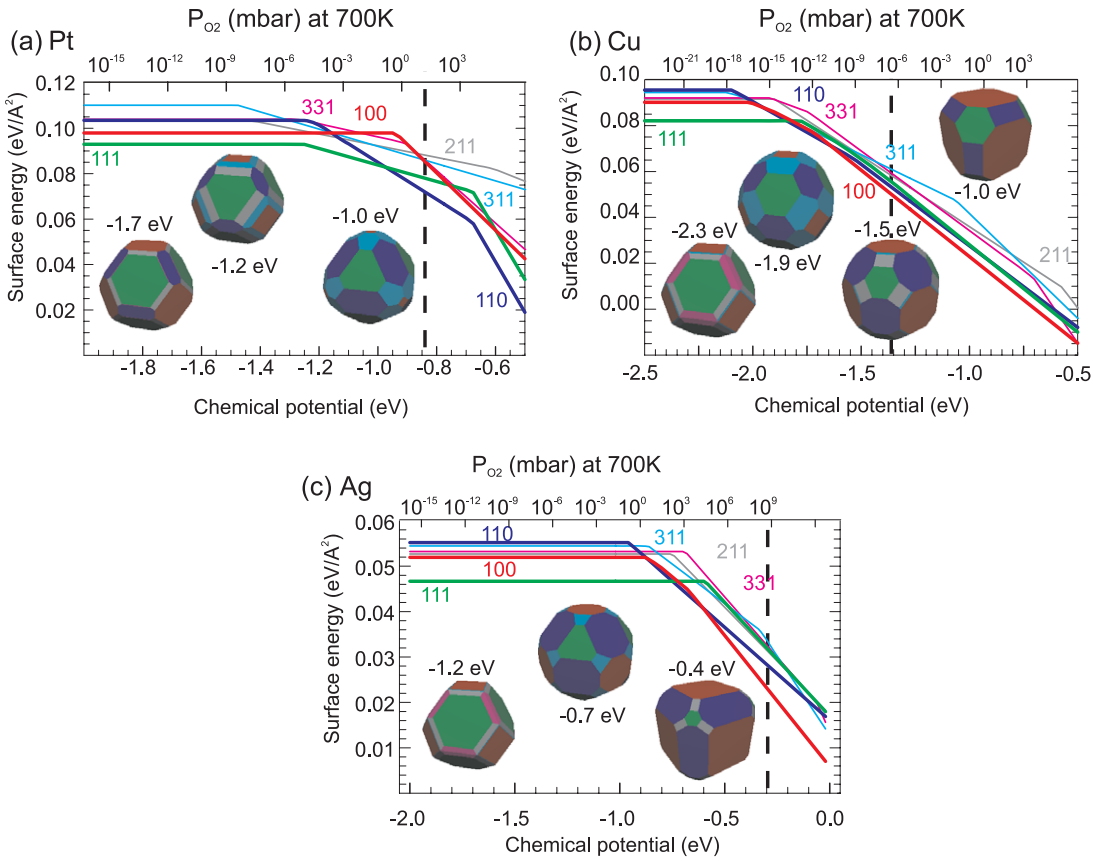

Figure 6. Comparative phase diagram of oxygen adsorption phases on different facet orientations and resulting particle shape of (a) platinum, (b) copper and (c) silver.

oxygen atoms experience a strong nearest-neighbor repulsion, which reduces the adsorption energy enough to suppress the formation of phases with a higher oxygen content (compare table 3). While oxygen shows a tendency to adsorb on the low-coordinated sites on the (311) surfaces of platinum group metals, the fourfold hollow adsorption site becomes more attractive on the noble metals Cu and Ag. This is also exemplified by the fact that the adsorption energies of a single oxygen atom on Cu(111) adsorbed in the threefold or fourfold hollow sites are degenerated. This facilitates the formation of the zig-zag structure mentioned before, where both sites are occupied. Consequently, on both noble metals the low-coverage adsorption of single oxygen atoms is only stable in a small regime of the chemical potential and changes readily into the higher-coverage structure. In addition, both surfaces are driven towards a missing-row reconstruction that facilitates the oxygen adsorption.

Adsorption on the (211) surfaces is very similar to that on the (311) surfaces, yet the steric restriction of the (311) surface is partially lifted as the (111) terrace is wider. This allows for structures similar to those discussed for the (331) surface. Independently of the step facet orientation, we find nearly the same adsorption energy on Rh(331), Rh(311) and Rh(211) (see table 3, 1O). This result can be explained by the similar adsorption site. The difference is more pronounced at a higher oxygen coverage, when the lower step edge is occupied. Both the zig-zag ('2O') structure as well as the fully covered step ('4O') are significantly less stable than their (331) counterparts. The same holds for Pd(311). On Pt(211), as on the shorter Pt(311), the adsorption energy for the bridge site at the step edge is strongly increased in the low-coverage case, leading to a suppression of the high-coverage structures. Opposite trends are predicted for Cu and Ag, where the higher affinity to the fourfold step facets stabilizes the structures at higher coverage.

3.3. Surface oxides and high-coverage reconstructions

At high chemical potentials, usually around values where bulk oxides become stable, the formation of surface oxides is experimentally observed. The surface oxides have a much higher oxygen density on the platinum-group metals than on the noble metals. This can be motivated by the fact that noble metals have no tendency to reach higher oxidation states; their bulk oxides have small enthalpies of formation and low oxygen content. Since the surface oxides are usually reminiscent of the respective bulk oxide and are therefore often similar on different facets of the same metal, in this subsection we group surfaces by metal, rather than by orientation as done in the previous subsections.

On Pt(111) an α-PtO_2 trilayer is the stable surface oxide [19, 70], for two reasons: α-PtO_2 is the stable bulk phase in oxygen at room temperature and atmospheric pressure [71, 19], and it consists of a layered structure similar to that of graphite, with sheets held together only by weak

van der Waals forces [19, 70]. Thus the isolated trilayer is itself very stable. Finally, the lattice mismatch is such that the trilayer can be accommodated on Pt(111) in a p(2 × 2) structure with negligible strain (Pt–Pt distances are increased in the trilayer by roughly 3% in comparison to bulk α-PtO_2). We have extended previous calculations [19] for surface oxides on Pt(100) in view of recent experimental results. While in [19] only PtO and Pt_3O_4 surface oxides had been considered, we have calculated also an α-PtO_2 trilayer on Pt(100) with (2 × 2) periodicity inspired by the fact that α-PtO_2 trilayers form on both Pt(111) and Pt(110). Upon relaxation, the trilayer moves to its stable configuration with two O atoms per cell on bridge positions between substrate Pt atoms and two O atoms on top. We find an interval of stability for both PtO-like and α-PtO_2 surface oxides, as shown in figure 2 together with the structure of the α-PtO_2 trilayer on Pt(100).

On Pt(110) a one-dimensional structure of oxide stripes with (12 × 2) periodicity has been observed and calculated [10, 72]. This structure has the same construction principle as (10 × 2) on Rh(110): the oxide stripes consist of oxygen atoms arranged on both sides of the Pt edge, with PtO_2 units missing in regular intervals to reduce the compressive stress. The (10× 2) structure lies only slightly higher in energy. At a chemical potential of about −0.7 eV there is a transition to an α-PtO_2 layer with a (2 × 4) periodicity, as shown in figure 3, which is different from the structure with (1 × 4) periodicity calculated by Li and co-workers [10]. The latter structure is highly stressed, as α-PtO_2 is compressed in one direction by 10%. We have managed to reduce the compression to less than 4% in our new model by rotating the oxide trilayer by 30° and allowing for double periodicity in that direction. This improves the energy drastically (see figure 3(a)). However, we believe this surface to be incommensurate with the substrate in the real system.

On Rh, as on Pt, basically the same oxide trilayer forms on the three low-index surfaces. On Rh(111) an O–Rh–O trilayer forms with a (9 × 9) periodicity [73]. On Rh(100) the surface oxide has a c(8 × 2) periodicity [74] and forms at a chemical potential of $\mu = -1.25$ eV. Also here, as on Rh(111) and Pd, the O atoms are located in an on-top position with respect to the substrate. On Rh(110) a striped (10 × 2) structure was found [75, 76], as well as a surface oxide with a trilayer structure as on Rh(111) and Rh(100) [7]. In [58] we calculated a small interval of stability for the one-dimensional (10 × 2) phase followed by a transition to the two-dimensional surface oxide.

On Pd surfaces, surface oxide structures are built from the same structural elements, namely Pd atoms linearly coordinated to two O atoms and Pd atoms square-planar coordinated to four O atoms, arranged in order to optimize interaction with the substrate: the Pd atoms are located in hollow sites of the underlying surface, the O atoms usually in on-top positions. On Pd(111) a characteristic 'Persian carpet' structure forms [77], with a Pd_5O_4 stoichiometry and no bulk correspondent. Near this stable structure a whole 'zoo' of six other metastable surface oxides has been observed [8]. In contrast to Pt and Rh, where all surface oxides consisted of the same structure derived from the bulk oxide, these structures are only loosely related to the bulk PdO structure. On Pd(100) a O–Pd–O trilayer forms [9, 78, 79], which corresponds to a bulk PdO(101) structure. On Pd(110) we found the (10 × 2) stripe structure to be stable [48], a fact which has not been verified experimentally yet. Few experiments exist in the high-coverage regime of this surface. Lundgren and co-workers [80] have found and characterized ($\sqrt{3}\times 7$) and ($\sqrt{3}\times 9$) structures, but they are only metastable according to *ab initio* calculations.

On the two noble metals considered, Ag and Cu, the highest O coverage attained experimentally is rather low, about 0.5 ML. At these levels heavily reconstructed structures have been observed, which display a high degree of similarity to Ag_2O and Cu_2O, respectively. Therefore, despite the low oxygen density, they have been sometimes dubbed as 'surface oxides', even if the metal–metal distances on the surface are those of the bulk metal [6]. On Ag(111) a p(4 × 4) phase has long been known to form under oxygen [11, 81, 82]; only recently has its atomic structure been unambiguously determined [12, 13]. This structure consists of triangles of six Ag atoms surrounded by six O atoms, with an O coverage of 3/8 ML. Ag atoms are linearly coordinated to two O atoms as in Ag_2O. Very recently, a new p(7 × 7) structure has been discovered on Ag(111), which resembles the p4 structures on Cu(111) [83]. On Ag(100) a p($2\sqrt{2}$ × 2)R45°-O phase forms [14, 84–86]. This structure has a coverage of 0.5 ML and is characterized by the oxygen atoms adsorbed in a c(2 × 2) overstructure, with each fourth Ag atom missing to accommodate the oxygen. Ag atoms in the topmost layer are linearly coordinated to two O atoms, thus reproducing the basic structural element of Ag_2O. The p($2\sqrt{2}$ × 2)R45°-O becomes thermodynamically stable at $\mu_O = -0.67$ eV, thus before bulk Ag_2O becomes stable (at −0.37 eV). As reported in the previous section, on Ag(110) there is a direct transition from the clean surface to a (1 × 2)-added row structure with an oxygen coverage of 0.5 ML (0.5 O atoms/(1 × 1) cell), as shown in figure 4. In this structure the basic O–Ag–O structural element derived from Ag_2O is again found. No other structures with high oxygen content have been observed on this facet.

On Cu(111) Cu_2O-like structures ('p4') have been observed [15], and the corresponding phase diagram has been calculated by Soon and co-workers [16]. The stable structures have a 4 × 4 periodicity and consist of Cu adatoms, each linearly coordinated to two oxygen atoms, arranged in a hexagonal configuration. A similar structure has been recently resolved experimentally on Ag(111) [83]. Due to the common properties of Ag(111) and Cu(111) we have also investigated a hypothetical p(4 × 4) structure (as discussed for Ag(111)) adsorbed on Cu(111), but it is energetically less stable than the 'p4' structures by 10 meV $Å^{-2}$. On Cu(100), the same reconstructed ($2\sqrt{2}$ × 2)R45°-O structure forms as on Ag(100) [17, 86–89]. This structure has the same oxygen content, 0.5 ML, as oxygen adsorbed in a simple c(2 × 2) structure with adsorbed oxygen. The latter structure is energetically slightly less favorable due to a higher surface stress [90], and thus metastable. Experimentally a c(2 × 2) structure has been observed on Cu(100) at low oxygen exposures and the ($2\sqrt{2}\times 2$)R45°-O sets in at higher exposures or higher temperatures [91, 92], suggesting kinetic hindrance

for its formation. On Cu(110) a c(6 × 2) structure (see figure 5(b)) was experimentally observed [93, 94], and the calculated phase diagram, shown in figure 5(a), supports the view that this is the stable phase at high oxygen chemical potentials. This phase has an oxygen coverage of 2/3 ML (eight O atoms in the c(6 × 2) cell), corresponding to ∼14.1 Å^2/O atom. This is higher than the O density of the surface oxides on Cu(111) (∼13.1 Å^2/O atom for the p4 + O_f structure) and Cu(100) (∼13.3 Å^2/O atom for the (2$\sqrt{2}$ × 2)R45°-O structure). The structure consists of Cu atoms linearly coordinated to two O atoms, in an arrangement related to the structure of bulk Cu_2O, with a $Cu_{10}O_8$ stoichiometry.

4. Particles

The detailed knowledge of the surface energies allows us to predict the thermodynamically stable particle shape by the Wulff construction as a function of the chemical potential. At a very low chemical potential of oxygen, corresponding to the low-pressure/high-temperature regime, the particle shape is dominated by the clean surfaces. As the ratios presented in this paper do not differ too much from those given by a bond-breaking model, the general appearance of all clean particles is quite similar. However, it must be stressed that no high-indexed (stepped) surfaces would appear in the Wulff shape if the surface energies followed exactly the bond-breaking model [48–50]. In the second regime oxygen adsorbs in low-coverage structures. As we have seen in the previous section, the average adsorption energies in these phases are generally proportional to the surface energy of the clean surface. Therefore the energetic difference between the respective surface orientations decreases, leading to a rounding of the particles. With increasing oxygen coverage, the average adsorption energy depends strongly on the adsorption phase present on the metal, leading to a less round particle shape. Finally, in the high-coverage regime surface oxides tend to form on the metal surface. These are only stable for selected surface orientations.

The results presented here for Pt, Ag, and Cu are to be compared to those in [48], where the morphology of Rh and Pd particles is discussed in detail.

Platinum has an exceptionally high surface energy for the ideal (100) and (110) surfaces (compare table 1), which would drastically decrease the corresponding exposed areas for the clean crystal. Yet both surfaces reconstruct, reducing the surface energy of these orientations, which results again in the truncated octahedral shape (figure 6(c), left particle). The energy cost to dereconstruct the surface implies that oxygen adsorption sets in rather late on Pt(100). On the other hand, the adsorption energy is especially high for the open (311) and (211) phases, and these facets are stabilized (figure 6(c), central particle). In the high-coverage regime, the PtO_2 surface oxide layers are—in contrast to Pd—only stable at a chemical potential beyond the stability of the bulk phase. Therefore, the highest oxygen content can be obtained by one-dimensional oxide stripes on Pt(110) and Pt(311), and a large proportion of the open (110) and (311) facets are displayed at a chemical potential of −1.0 eV.

The shape of clean Cu particles is again a truncated octahedron, with additional (331) and (211) decorations between the (111) and (100) facets, respectively. But in contrast to the platinum-group metals, on Cu(110) a very stable added-row reconstructed surface forms at intermediate chemical potential. In addition, also the adsorption on the surface with the second highest surface energy, the (missing-row reconstructed) Cu(311), is quite favorable. Therefore, in the initial oxidation phase large areas of (110) and (311) facets are exposed. At increasing partial pressure of oxygen the difference in the free surface energies becomes very small, leading again to a rounded crystal at a chemical potential of −1.5 eV (figure 6(d)). In the high-coverage case, the shape of the Cu particles is dominated by the Cu(100) p(2$\sqrt{2}$ × 2) adsorption structure.

In the case of silver, the surfaces energies are far lower than for the transition metals. Yet the ratio between the respective facet orientations (compare table 2) results in the same shape for the clean particles as predicted for the other crystals. As in the case of Cu, oxygen adsorption sets in on the added-row reconstructed Ag(110) facets, leading to a pronounced exposure of those facets in the low-coverage regime (figure 6(e)). At increasing oxygen partial pressure, only oxygen adsorbed on the Ag(100) facets becomes competitive, resulting in a particle shape dominated by (110) and (100) areas. It is important to realize that the commonly studied Ag(111) facet is strongly diminished at high pressures.

5. Discussion

As the reactivity of the metal particles depends on the exposed surface orientations, we discuss the implications of our results for oxidation catalysis in the following section. Although nowadays it has become feasible to study the catalytic activity for a particular reaction on a selected surface orientation by combining *ab initio* data with kinetic Monte Carlo simulations [23], the vast amount of required calculations makes a systematic evaluation of general trends in the late transition metals impractical. Therefore, simple descriptors are still commonly used. One of the oldest descriptors is based on Sabatier's principle [95], established almost a century ago. According to this principle, the best catalysts are those on which the dissociation products are neither too strongly nor too weakly bound. This is related to the Brønsted–Evans–Polanyi relation [96, 97], which states that for many reactions the enthalpy barrier for the dissociation of the reactants is a linear function of the adsorption energy of the dissociation products [98, 99]. Thus the intermediate adsorption energies of the best catalysts are a compromise between the need for low dissociation barriers and low adsorption energies. As a consequence, the oxygen adsorption energy is a good indicator of the catalytic activity for total oxidation catalysis. Nørskov and co-workers analyzed this behavior in detail by considering a kinetic model, and found a dependence of the maximum in turnover rates on the reaction energy for the dissociative chemisorption of the reactants [100]. The exact position of this maximum depends also on a number of parameters, such as the temperature or the mechanism of the reaction. Yet, for

Table 4. Stable adsorption phases of oxygen on Ag and Cu surfaces. The adsorption energies are given with respect to the unreconstructed surface. Missing-row reconstructed structures are indicated by (MR). For stepped surfaces, low-coverage oxygen adsorption is indicated as 1O, '*p2mg*'-like structures as 2O, and oxide stripes as 4O.

Structure	E_{ads} (eV)	Structure	E_{ads} (eV)
Ag(111) p(4 × 4)	−0.59	Ag(100) p(2 × 2)	−0.88
Ag(100) c(4 × 6)	−0.86	Ag(100) p(2$\sqrt{2}$ × 2)R45°-O	−0.80
Ag(110) (2 × 1)-added row	−0.96	Ag(331) 1O	−0.65
Ag(331) 2O	−0.69	Ag(331) 4O	−0.37
Ag(311) 2O (MR)	−0.87	Ag(311) 2O	−0.60
Ag(211) 1O	−0.68	Ag(211) 2O	−0.75
Cu(111) p4-CuO_3	−1.78	Cu(111) p4	−1.76
Cu(111) p4 + O_f	−1.71	Cu(100) p(2 × 2)	−2.01
Cu(100) c(4 × 6)	−1.98	Cu(100) p(2$\sqrt{2}$ × 2)R45°-O	−1.89
Cu(110) (2 × 1)-added row	−2.11	Cu(110) c(6× 2)	−1.97
Cu(110) (10 × 2)	−1.53	Cu(331) 1O	−1.92
Cu(331) 2O	−1.83	Cu(331) 4O	−1.27
Cu(311) 1O (MR)	−2.04	Cu(311) 2O (MR)	−2.06
Cu(211) 1O	−1.86	Cu(211) 2O	−1.90
Cu(211) 4O	−1.24		

many processes the optimal value of the dissociative adsorption energy varies between −1 and −3 eV. Of all the transition metals presented in this paper, only Ag surfaces display a weaker oxygen adsorption (see table 4), which is consistent with the fact that this metal is not applicable for total oxidation reactions. Still, it is important to notice that the commonly considered oxygen adsorption energies are those for the low-coverage cases, while the phase diagrams presented in this paper clearly indicate that surfaces often tend to form high-coverage phases under catalytic conditions. If the oxygen pressure is high enough to lead to the formation of a surface oxide, the chemical properties of the surface are rather related to that of the respective oxide. The differences in catalytic activity between Rh and Cu illustrate this: while the two metals have similar adsorption energies on the metal surfaces (see tables 3 and 4), their respective oxides have completely different stoichiometries and structures (Cu_2O, CuO versus Rh_2O_3) and certainly different adsorption properties for gas species. This is probably one of the reasons why rhodium cannot be substituted by the cheaper copper in oxidation catalysts, and this shows once more that studies under UHV are not sufficient to understand the functionality of these materials at realistic pressures.

A detailed analysis of our data of the oxygen adsorption energies shows a correlation between the surface energy and the low-coverage adsorption energy. A linear relation between the surface energy γ and the low-coverage adsorption energy E_{ads} has been established for Rh and Pd surfaces in [48], thus giving a quantitative basis to the common idea that an 'open' surface yields a higher adsorption energy. If this kind of analysis is extended to a wider selection of transition metals (table 5), a more complex picture arises. On closer inspection it becomes evident that the common notion that an 'open' surface yields a higher adsorption energy still holds, but cannot be summarized with one universal scaling factor. Yet, for the 4d metals we still find strong similarities. The average ratios $\frac{\gamma}{E_{ads}}$ for Rh and Pd are nearly identical, 0.065 and 0.066 Å^{-2} respectively, while Ag has mean value of 0.069. It should also be noticed that the standard deviation of the ratio for Rh and Pd is less than 4%, while for Ag it is as high as 13% (see table 5).

Table 5. Ratio γ/E_{ads} between surface energies and low-coverage oxygen adsorption energies (in Å^{-2}). For platinum, the values marked with an asterisk are given with respect to the unreconstructed surface. For each metal, σ is the standard deviation of the average.

Surface	Rh	Pd	Ag	Cu	Pt
(111)	0.060	0.062	0.079	0.046	0.074
(100)	0.067	0.068	0.060	0.045	0.085*
(110)	0.065	0.064	0.058	0.046	0.085*
(311)	0.068	0.068	0.062	0.046	0.075*
(331)	0.065	0.066	0.077	0.048	0.082
(211)	0.065	0.070	0.077	0.049	0.072
Average	0.065	0.066	0.069	0.049	0.079
σ	0.003	0.003	0.009	0.002	0.006

For the 3d metal Cu we find a much smaller mean value of 0.046, and for the 5d metal Pt by far the highest mean ratio of 0.079, with standard deviations of 4% and 8%, respectively. In spite of the larger deviations for Ag and Pt, we therefore see that the linear correlation is at least fulfilled for each single row of the periodic table separately. The detailed knowledge of the Gibbs free surface energies for different chemical potentials allows us to evaluate the corresponding Wulff shape. Thus the information about the stability of the adsorption phases allows us to predict which of the facets are exposed. The comparison between the transition metals shows common aspects. The shape of the clean particles is a truncated octahedron with large areas of (111) and (100) facets, decorated with high-index surfaces such as (331) and (311). The presence of the latter facets is only made possible by deviations of the surface energies from those of a bond-breaking model. This common picture continues after the onset of oxygen adsorption. Since the oxidation starts at the open surfaces, they are stabilized in comparison with the (111) surface. The difference in surface energies decreases, resulting in a rounder particle shape. While this effect is pronounced for Pt and Cu, the (111) surface is still dominant for Rh and Pd. Finally, when the chemical potential approaches the stability of the bulk oxide regime, surface

oxides form. For Rh and Pt, the structure of the surface oxide is basically independent of the surface orientation and consists of an α-PtO_2-like layer. On the other hand, on Pd the surface oxides display a larger variety of structures, with considerable surface areas of both Pd(111) and Pd(100) exposed. Finally, for both noble metals, Ag and Cu, we predict the presence of large (100) areas on the particle surface at high chemical potential, with additional contributions of (111) and (110) areas.

We believe that controlling the equilibrium particle shape is an important first step towards understanding of particle morphology in a realistic environment. Unfortunately, apart from the work of Henry and co-workers [25, 28] for Pd particles, we are not aware of experiments systematically investigating the equilibrium shape changes as a function of the oxygen chemical potential for these metals.

Moreover, the calculations predict stability of phases which have not yet been observed experimentally: the adsorption in a c(4 × 6) structure on Cu(100), which was observed only on Ag(100), and the α-PtO_2 trilayer on Pt(100), the existence of which was only hinted at but not atomically resolved [18]; finally, for the α-PtO_2 trilayer on Pt(110) we have proposed an improved model with (2 × 4) periodicity instead of the (1 × 4) periodicity originally proposed by Hammer and co-workers [10]. However, we believe that the α-PtO_2 trilayer might build an incommensurate surface oxide on these facets. Moreover, our results on Pt(100) show that both a PtO-like monolayer and an α-PtO_2 surface oxide are thermodynamically stable, though at different chemical potentials. This is in agreement with the fact that the oxide formed on this surface is similar to that built on Pt(111) [18], suggesting an α-PtO_2 surface oxide. As for Ag and Cu, the known phases have a low oxygen coverage and a high number of metal–metal bonds on the surface, so that they are sometimes not even considered to be 'true surface oxides' [12]. The difference is apparent for the (111) facets: while on platinum-group metals oxygen adsorption sets in with simple chemisorption, on the two noble metals there is a direct transition (at much higher chemical potentials) to reconstructed phases with undercoordinated metal atoms. These phases become stable before the onset of stability of the respective bulk oxides.

6. Summary

We have studied the oxidation of the low-index as well as selected stepped surfaces of several platinum-group and noble metals, that is Pt, Rh, Pd, Ag and Cu. The surface energies of the bare surfaces are described within 8% accuracy by a bond-breaking model. We predict the stability of novel phases, namely the adsorption structure c(4 × 6) on Cu(100) and the α-PtO_2 trilayer on Pt(100). For the α-PtO_2 trilayer on Pt(110) we have proposed an improved model with (2 × 4) periodicity, though the oxide will probably be incommensurate with respect to the substrate. The ratios γ/E_{ads} between the surface energy of the bare surface γ and the oxygen adsorption energy at low oxygen coverage E_{ads} are roughly constant within one row of the periodic table. Finally, the particle shapes have been predicted as a function of the oxygen chemical potential by a Wulff construction. Clean particles have the shape of a truncated octahedron decorated by stepped surfaces; oxygen adsorbs first on the more open surfaces, leading to a rounding of the crystallite at intermediate chemical potentials. At high chemical potentials, the formation of surface oxides leads to a predominance of the facets where the surface oxides are most stable: (111) and (110) for platinum, and (100) for silver and copper. Only a few experiments exist that address the particle shape in thermodynamic equilibrium with an oxygen-rich environment. We believe this to be a first important step towards understanding of particle morphology in a realistic environment, and we hope that this article will stimulate further research in this field.

Acknowledgments

We would like to thank Georg Kresse for fruitful discussions. This work was financially supported by the Austrian Fonds zur Förderung der wissenschaftlichen Forschung (FWF) and the European Union under Contract No. NMP3-CT-2003-505670 (NANO2).

References

[1] Hodnett B K 2000 *Heterogeneous Catalytic Oxidation* (Chichester: Wiley)
[2] Gandhi H S, Graham G W and McCabe R W 2003 *J. Catal.* **216** 433
[3] Williams F J, Palermo A, Tikhov M S and Lambert R M 2001 *J. Phys. Chem.* B **105** 1381
[4] van Santen R A and Kuipers H P C E 1987 *Adv. Catal.* **35** 265
[5] Magaeva A A, Shmotin V S, Vodyankina O V, Knyazev A S, Salanov A N, Chesalov Yu A, Stoyanov E S, Odegova G V and Kurina L N 2006 *Russ. J. Phys. Chem.* **80** 706
[6] Lundgren E, Mikkelsen A, Andersen J N, Kresse G, Schmid M and Varga P 2006 *J. Phys.: Condens. Matter* **18** R481
[7] Dudin P, Barinov A, Gregoratti L, Kiskinova M, Esch F, Dri C, Africh C and Comelli G 2005 *J. Phys. Chem.* B **109** 13649
[8] Klikovits J, Napetschnig E, Schmid M, Seriani N, Dubay O, Kresse G and Varga P 2007 *Phys. Rev.* B **76** 45405
[9] Kostelník P, Seriani N, Kresse G, Mikkelsen A, Lundgren E, Blum V, Šikola T, Varga P and Schmid M 2007 *Surf. Sci.* **601** 1574
[10] Li W X, Österlund L, Vestergaaard E K, Vang R T, Matthiesen J, Pedersen T M, Lægsgaard E, Hammer B and Besenbacher F 2004 *Phys. Rev. Lett.* **93** 146104
[11] Rovida G, Pratesi F, Maglietta M and Ferroni E 1972 *J. Vac. Sci. Technol.* **9** 796
[12] Schmid M *et al* 2006 *Phys. Rev. Lett.* **96** 146102
[13] Schnadt J, Michaelides A, Knudsen J, Vang R T, Reuter K, Lægsgaard E, Scheffler M and Besenbacher F 2006 *Phys. Rev. Lett.* **96** 146101
[14] Costina I, Schmid M, Schiechl H, Gajdoš M, Stierle A, Kumaragurubaran S, Hafner J, Dosch H and Varga P 2006 *Surf. Sci.* **600** 617
[15] Matsumoto T, Bennett R A, Stone P, Yamada T, Domen K and Bowker M 2001 *Surf. Sci.* **471** 225
[16] Soon A, Todorova M, Delley B and Stampfl C 2006 *Phys. Rev.* B **73** 165424
[17] Mayer R, Zhang C-S and Lynn K G 1986 *Phys. Rev.* B **33** 8899
[18] Shumbera R B, Kan H H and Weaver J F 2007 *Surf. Sci.* **601** 235

[19] Seriani N, Pompe W and Ciacchi L C 2006 *J. Phys. Chem.* B **110** 14860
[20] Ackermann M D *et al* 2005 *Phys. Rev. Lett.* **95** 255505
[21] Hendriksen B M L and Frenken J W M 2002 *Phys. Rev. Lett.* **89** 46101
[22] Mars P and van Krevelen D W 1954 *Chem. Eng. Sci.* **3** 41
[23] Rogal J, Reuter K and Scheffler M 2007 *Phys. Rev. Lett.* **98** 46101
[24] Qu Z, Cheng M, Huang W and Bao X 2005 *J. Catal.* **229** 446
[25] Graoui H, Giorgio S and Henry C R 1998 *Surf. Sci.* **417** 350
[26] Schalow T, Brandt B, Starr D E, Laurin M, Schauermann S, Shaikhudtinov S K, Libuda J and Freund H J 2006 *Catal. Lett.* **107** 189
[27] Marks L D 1994 *Rep. Prog. Phys.* **57** 603
[28] Graoui H, Giorgio S and Henry C R 2001 *Phil. Mag.* **81** 1649
[29] Silly F and Castell M R 2005 *Phys. Rev. Lett.* **94** 46103
[30] Hoefelmeyer J D, Niesz K, Somorjai G A and Tilley T D 2005 *Nano Lett.* **5** 435
[31] Hansen K H, Worren T, Stempel S, Lægsgaard E, Baumer M, Freund H J, Besenbacher F and Stensgaard I 1999 *Phys. Rev. Lett.* **83** 4120
[32] Chapon C, Granjeaud S, Humbert A and Henry C R 2001 *Eur. Phys. J. AP* **13** 23
[33] Kasper N, Stierle A, Nolte P, Jin-Phillipp Y, Wagner T, de Oteyza D G and Dosch H 2006 *Surf. Sci.* **600** 2860
[34] Kresse G and Hafner J 1993 *Phys. Rev.* B **47** 558
[35] Blöchl P E 1994 *Phys. Rev.* B **50** 17953
[36] Kresse G and Joubert D 1999 *Phys. Rev.* B **59** 1758
[37] Perdew J P, Chevary J A, Vosko S H, Jackson K A, Pederson M R, Singh D J and Fiolhais C 1992 *Phys. Rev.* B **46** 6671
[38] Monkhorst H J and Pack J D 1976 *Phys. Rev.* B **13** 5188
[39] Reuter K and Scheffler M 2001 *Phys. Rev.* B **65** 35406
Reuter K and Scheffler M 2007 *Phys. Rev.* B **75** 49901 (erratum)
[40] Wulff G 1901 *Z. Kristallogr.* **34** 445
[41] Campbell C T, Parker S C and Starr D E 2002 *Science* **298** 811
[42] Reinhard D, Hall B D, Berthoud P, Valkealahti S and Monot R 1997 *Phys. Rev. Lett.* **79** 1459
[43] Vitos L, Ruban A V, Skriver H L and Kollar J 1998 *Surf. Sci.* **411** 186
[44] Kwon S K, Nabi Z, Kadas K, Vitos L, Kollar J, Johansson B and Ahuja R 2005 *Phys. Rev.* B **72** 235423
[45] Yu B D and Scheffler M 1996 *Phys. Rev. Lett.* **77** 1095
[46] Galanakis I, Papanikolaou N and Dederichs P H 2002 *Surf. Sci.* **511** 1
[47] Galanakis I, Bihlmayer G, Bellini V, Papanikolaou N, Zeller R, Blügel S and Dederichs P H 2002 *Europhys. Lett.* **58** 751
[48] Mittendorfer F, Seriani N, Dubay O and Kresse G 2007 *Phys. Rev.* B **76** 233413
[49] Frenken J W M and Stoltze P 1999 *Phys. Rev. Lett.* **82** 3500
[50] Desjonquères M C, Spanjaard D, Barreteau C and Raouafi F 2002 *Phys. Rev. Lett.* **88** 56104
[51] Kellogg G L 1985 *Phys. Rev. Lett.* **55** 2168
[52] Heinz K, Lang E, Strauss K and Müller K 1982 *Surf. Sci.* **120** L401
[53] Heilmann P, Heinz K and Müller K 1979 *Surf. Sci.* **83** 487
[54] Van Hove M A, Koestner R J, Stair P C, Biberian J P, Kesmodel L L, Bartoš I and Somorjai G A 1981 *Surf. Sci.* **103** 189
[55] Alfe D, de Gironcoli S and Baroni S 1998 *Surf. Sci.* **410** 151
[56] Baraldi A, Cerda J, Martin-Gago J A, Comelli G, Lizzit S, Paolucci G and Rosei R 1999 *Phys. Rev. Lett.* **82** 4874
[57] Deskins N A, Lauterbach J and Thomson K T 2005 *J. Chem. Phys.* **122** 184709
[58] Dri C, Africh C, Esch F, Comelli G, Dubay O, Köhler L, Mittendorfer F and Kresse G 2006 *J. Chem. Phys.* **125** 094701
[59] Comelli G, Dhanak V R, Kiskinova M, Prince K C and Rosei R 1998 *Surf. Sci. Rep.* **32** 165
[60] Comelli G, Dhanak V R, Kiskinova M, Paolucci G, Prince K C and Rosei R 1992 *Surf. Sci.* **269/270** 360
[61] Murray P W, Leibsle F M, Li Y, Guo Q, Bowker M, Thornton G, Dhanak V R, Prince K C and Rosei R 1993 *Phys. Rev.* B **47** 12976
[62] Dhanak V R, Prince K C, Rosei R, Murray P W, Leibsle F M, Bowker M and Thornton G 1994 *Phys. Rev.* B **49** 5585
[63] Ertl G and Rau P 1969 *Surf. Sci.* **15** 443
[64] Yagi K and Fukutani H 1998 *Surf. Sci.* **412/413** 489
[65] Nishijima M, Jo M, Kuwahara Y and Onchi M 1986 *Solid State Commun.* **60** 257
[66] Kralj M, Pertram T, Seriani N, Becker C, Krupski A, Mittendorfer F, Kresse G and Wandelt K 2007 at press
[67] Brena B, Comelli G, Ursella L and Paolucci G 1997 *Surf. Sci.* **375** 150
[68] Gustafson J *et al* 2006 *Phys. Rev.* B **74** 035401
[69] Klikovits J, Schmid M and Varga P 2007 at press
[70] Li W X and Hammer B 2005 *Chem. Phys. Lett.* **409** 1
[71] Muller O and Roy R 1968 *J. Less-Common Met.* **16** 129
[72] Pedersen T M, Li W X and Hammer B 2006 *Phys. Chem. Chem. Phys.* **8** 1566
[73] Gustafson J *et al* 2004 *Phys. Rev. Lett.* **92** 126102
[74] Gustafson J *et al* 2005 *Phys. Rev.* B **71** 115442
[75] Vesselli E, Africh C, Baraldi A, Comelli G, Esch F and Rosei R 2001 *J. Chem. Phys.* **114** 4221
[76] Africh C, Esch F, Comelli G and Rosei R 2001 *J. Chem. Phys.* **115** 477
[77] Lundgren E, Kresse G, Klein C, Borg M, Andersen J N, De Santis M, Gauthier Y, Konvicka C, Schmid M and Varga P 2002 *Phys. Rev. Lett.* **88** 246103
[78] Todorova M *et al* 2003 *Surf. Sci.* **541** 101
[79] Zheng G and Altman E I 2002 *Surf. Sci.* **504** 253
[80] Westerström R, Weststrate C J, Resta A, Andersen J N, Lundgren E, Stierle A, Schmid M, Seriani N, Mittendorfer F and Kresse G 2007 at press
[81] Rovida G, Pratesi F, Maglietta M and Ferroni E 1974 *Surf. Sci.* **43** 230
[82] Campbell C T 1985 *Surf. Sci.* **157** 43
[83] Reicho A, Stierle A, Costina I and Dosch H 2007 *Surf. Sci.* **601** L19
[84] Loffreda D, Dal Corso A, Baroni S, Savio L, Vattuone L and Rocca M 2004 *Surf. Sci.* **539** 26
[85] Rocca M *et al* 2000 *Phys. Rev.* B **61** 213
[86] Bonini N, Kokalj A, Dal Corso A, de Gironcoli S and Baroni S 2006 *Surf. Sci.* **600** 5074
[87] Wöll C, Wilson R J, Chiang S, Zeng H C and Mitchell K A R 1990 *Phys. Rev.* B **42** 11926
[88] Wuttig M, Franchy R and Ibach H 1989 *Surf. Sci.* **213** 103
[89] Zeng H C, McFarlane R A and Mitchell K A R 1989 *Surf. Sci.* **208** L7
[90] Harrison M J, Woodruff D P, Robinson J, Sander D, Pan W and Kirschner J 2006 *Phys. Rev.* B **74** 165402
[91] Richter H and Gerhardt U 1983 *Phys. Rev. Lett.* **51** 1570
[92] Mattsson A, Panas I, Siegbahn P, Wahlgren U and Åkeby H 1987 *Phys. Rev.* B **36** 7389
[93] Ertl G 1967 *Surf. Sci.* **6** 208
[94] Feidenhans'l R, Grey F, Johnson R L and Nielsen M 1991 *Phys. Rev.* B **44** 1875
[95] Sabatier P 1920 *La Catalyse en Chimie Organique* (Paris: Berange)
[96] Brønsted N 1928 *Chem. Rev.* **5** 231
[97] Evans M G and Polanyi M 1938 *Trans. Faraday Soc.* **34** 11
[98] Nørskov J K *et al* 2002 *J. Catal.* **209** 275
[99] Michaelides A, Liu Z P, Zhang C J, Alavi A, King D A and Hu P 2003 *J. Am. Chem. Soc.* **125** 3704
[100] Bligaard T, Nørskov J K, Dahl S, Matthiesen J, Christensen C H and Sehested J 2004 *J. Catal.* **224** 206